

Insulating behavior at the neutrality point in dual-gated, single-layer graphene

F. Amet,¹ J. R. Williams,² K. Watanabe,³ T. Taniguchi,³ and D. Goldhaber-Gordon²

¹*Department of Applied Physics, Stanford University, Stanford, CA 94305, USA*

²*Department of Physics, Stanford University, Stanford, CA 94305, USA*

³*Advanced Materials Laboratory, National Institute for Materials Science, 1-1 Namiki, Tsukuba, 305-0044, Japan*

The fate of the low-temperature conductance at the charge-neutrality (Dirac) point in a single sheet of graphene is investigated down to 20 mK. The potential fluctuations in graphene are made artificially small by using a dual top- and back-gate geometry such that screening reduces the intrinsic disorder potential. As the temperature is lowered, the peak resistivity diverges with a power-law behavior and becomes as high as several Megaohms per square at the lowest temperature, in contrast with the commonly observed saturation of the conductivity. As a transverse magnetic field is applied, our device remains insulating and directly transitions to the $\nu=0$ quantum Hall state at a field of 100 mT.

The ability to create electronic devices in graphene has made it possible to study 2D Dirac fermions in the solid state [1–3]. Transport measurements in a large magnetic field display quantum Hall plateaus with unconventional values of conductance, a signature of the Dirac equation describing electrons in graphene [1]. Such behavior emerges as the cyclotron gap opens in a magnetic field: when this gap becomes larger than disorder-induced fluctuations in the surrounding potential, the effect of the linear Dirac band structure becomes evident. At zero magnetic field, the disorder landscape dominates [4, 30], blurring the interesting phenomena that might occur at the Dirac point. Recently, the influence of disorder has been reduced by either suspending a sheet [5] or placing it on atomically-flat boron nitride [6], and many discoveries in transport have been made due to the more readily-accessible Dirac point in these cleaner systems [7–10].

The nature of the conductivity at the charge-neutrality point σ_{NP} has been debated since the first graphene-based devices were fabricated. Theory for ballistic graphene predicts a value of $4e^2/\pi h$ for σ_{NP} [11, 12]. However, early experiments on graphene measured σ_{NP} in the range of $2\text{--}12 e^2/h$ [2, 13, 14]. It was soon realized that σ_{NP} was sample-dependent and determined by the density of carriers in electron and hole puddles due to disorder from static charges on or near the sheet of graphene [13, 15, 16]. In suspended graphene devices [15] the conductivity showed a more pronounced temperature dependence, but still saturated at low temperature and remained higher than $4e^2/\pi h$. Recently it has been shown that the potential landscape in graphene can be made artificially clean by screening potential fluctuations with a second nearby, doped graphene sheet [17]. In that work, instead of saturating at values near e^2/h , σ_{NP} dropped with a power-law temperature dependence T^α , where $\alpha=2$ for the most insulating samples, down to $T=4\text{ K}$. Further, the authors observed a strong magnetoresistance in the temperature regime above 10 K and attributed it to weak localization, inferring that ultra-clean graphene may be an Anderson insulator. However, a recent theory [18] postulates that this temperature de-

pendence results from a “disorder by order” effect in graphene, where increasing order causes the sample to become more insulating at low density. Here $\sigma_{NP} \propto T^\alpha$ naturally emerges as the temperature dependence of conduction through a landscape of electron and hole puddles. To distinguish between the two competing scenarios, lower-temperature transport, where the electronic coherence important in localization is more prominent, is needed.

In this Letter, we report on electronic transport in dual-gated, single-layer graphene devices, in which the back gate is used to control the global carrier density, and the top gate is primarily used to screen the Coulomb disorder potential, not to locally control the carrier density. At the charge neutrality point (CNP), the dependence of the conductance g_{NP} on temperature (T) and magnetic field (B) is investigated down to temperatures of 20 mK. The temperature dependence is strong down to $T=400\text{ mK}$ and can be fitted to a power-law $g_{NP} \propto T^\alpha$ with $\alpha \approx 0.48 \pm 0.05$. The low-field magnetoresistance shows an uncommon behavior around $B=0$ that is inconsistent with weak localization. The quantum Hall regime is entered at just 0.1 T, but instead of showing a conductance plateau at $2e^2/h$ around the CNP, the device is insulating, indicating that the spin and valley SU(4) symmetry is broken at very low fields. A peak in $g_{NP}(B)$ marks a transition between the zero field insulating state and the $\nu=0$ insulator at a field on order 100 mT, about 20 times lower than for our non top-gated devices. From the low-temperature saturation of $g_{NP}(T)$ and the field at which the $\nu=0$ quantum Hall plateau emerges, we estimate that the potential fluctuations are less than $100\text{ }\mu\text{eV}$, an order of magnitude lower than reported for the suspended devices.

We fabricated our devices using hexagonal-boron nitride (h-BN) as a substrate for graphene, with good electronic properties [6, 19] resulting from the extreme flatness and cleanliness of h-BN flakes. Single-layer graphene flakes were exfoliated on a stack of polyvinyl alcohol (PVA) and polymethyl-methacrylate (PMMA). Separately, h-BN was exfoliated on a silicon wafer with

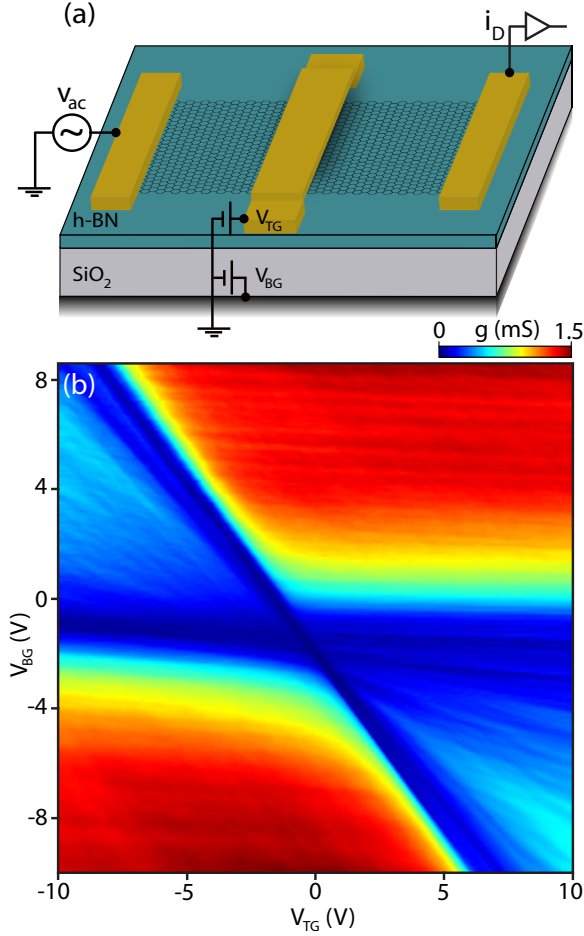


FIG. 1: (a) Schematic of the device in voltage biased mode. A bias v_{AC} is applied to the sample, the current i_D is then collected at the drain and measured with a lock-in amplifier. A voltage V_{BG} is applied to the degenerately doped piece of wafer to control the carrier density in the whole sheet. V_{TG} is applied to a suspended metallic gate, 70nm away from the graphene sheet, which varies the carrier density underneath it. (b) Conductivity σ as a function of both gate voltages, measured at a temperature $T=4$ K.

a 300 nm-thick thermal oxide, then exposed to flowing Ar/O_2 at 500°C for 8 hours, which removes organic contamination from tape residue [21, 22]. Each flake was characterized by atomic force microscopy and Raman spectroscopy prior to transfer [20]. The PVA layer was dissolved in deionized water, which lifted off the PMMA membrane with the attached graphene flake [6]. The graphene flake was then aligned to the h-BN, pressed on top and baked at 110°C to promote adhesion between the two flakes. The PMMA membrane was dissolved in acetone/IPA and the graphene/h-BN stack was again treated in Ar/O_2 at 500°C for 4 hours [21]. The cleanliness of the whole stack was confirmed with Raman spectroscopy [20]. Successive electron-beam lithography steps were used to oxygen-etch the graphene flake into a Hall-bar and to make electrical contact to the device (1 nm Cr, 200 nm Au). Finally, a $1\ \mu\text{m}$ wide top gate, also

patterned by electron-beam lithography, was suspended 70 nm above the flake [23–26]. For a last cleaning step, we could not anneal the device in oxygen, as we found it damages the metallic contacts [21]. Instead, the device was annealed at 325°C in Ar/H_2 for 4 hours. Additional details on the fabrication and characterization are available in Ref. [20]. A schematic of the completed device geometry is shown in Fig. 1(a). Another device, called the control device, was fabricated with no top-gate on the same sheet of graphene but electrically isolated from the top-gated device. The control device showed none of the distinct transport properties of the top-gated device at the CNP, helping discern which transport features are solely due to the presence of the suspended gate.

Graphene devices were measured in two different cryostats: a variable-temperature insert enabling temperature-dependent transport measurements from 300 K down to 1.7 K, and a dilution fridge where samples were measured at lower temperatures, down to 20 mK. The conductance g is determined in a standard voltage-biased lock-in measurement with an excitation voltage of $4\ \mu\text{V}$ at 92.3Hz. The resistance r is defined as $1/g$. DC voltages are applied to the top-gate (V_{TG}) and back-gate (V_{BG}).

g is shown on Figure 1(b) as a function of V_{TG} and V_{BG} at $T=4$ K. The carrier density can be controlled independently and with opposite polarities underneath and outside the top-gated region. As in previous work on dual-gated graphene [3, 27, 28], g exhibits local minima along two intersecting lines corresponding to each region being tuned through the CNP. However, unlike in typical dual-gated graphene devices, g_{NP} is near zero along these lines. g was also measured in a 4-probe geometry, from which we extracted the resistance of the cryostat's wiring, 2.5 k Ω . Underneath the top-gate, $C_{TG}V_{TG} + C_{BG}V_{BG} = 0$ at the CNP, yielding a top-gate-to-back-gate capacitance ratio of 1.3 from the slope of the diagonal line in the (V_{BG}, V_{TG}) plane. C_{BG} is $5.94(\pm 0.5) \times 10^{10} \text{ cm}^{-2} \text{ V}^{-1}$, as extracted from the periodicity of Shubnikov-de-Haas oscillations. Using a parallel-plate capacitance model, we estimate that the top gate is 70 nm away from the flake, which was confirmed by atomic force microscopy. The device exhibits little intrinsic doping, with a CNP voltage of -2.2 V on the back-gate, and a mobility of $60,000 \text{ cm}^2/\text{Vs}$, as extracted from a linear fit to $g(V_{BG})$ at the CNP. We note that the mobility of top-gated and non top-gated regions was comparable, which shows that the suspended gate does not deteriorate the electronic properties of our device.

Unlike typical graphene samples, r as a function of V_{BG} has a strong temperature dependence in our device (all measurements from here on are taken with $V_{TG}=0$). The resistance at the CNP r_{NP} dramatically increases at low temperature, from 13 k Ω at $T=300$ K to 300 k Ω at $T=4$ K [inset, Fig. 2(a)]. By contrast, the peak in r of the control device is only 10 k Ω at 4 K [20], comparable

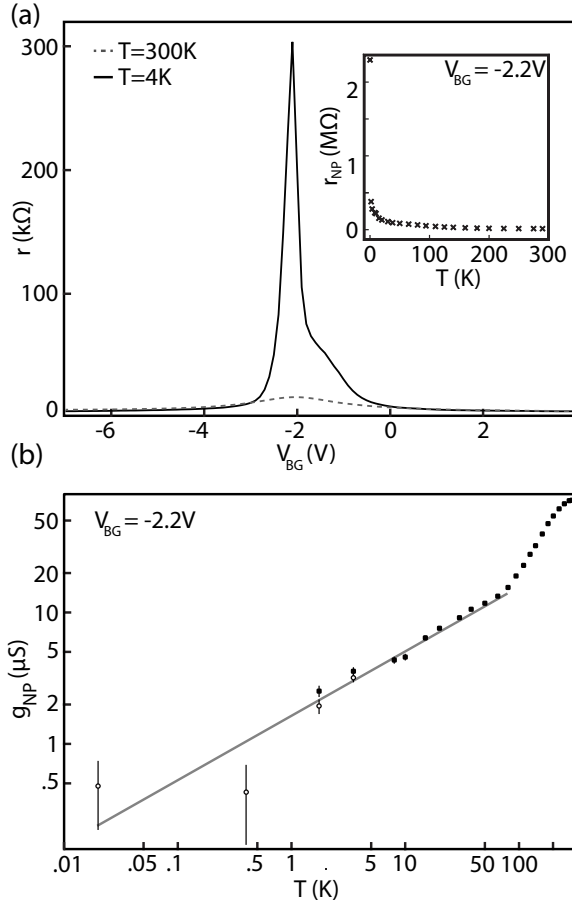


FIG. 2: (a) Resistance as a function of V_{BG} at $T=300\text{K}$ (dashed grey line) and $T=4\text{K}$ (black line). Inset: Resistance at the charge neutrality point ($V_{BG} = -2.2\text{V}$) as a function of temperature. (b) Conductance as a function of temperature on a log scale, at $V_{BG} = -2.2\text{V}$. Open circles and filled squares correspond to data points taken in the dilution fridge and variable temperature cryostat respectively. Error bars correspond to one standard deviation: for $T > 5\text{K}$, these are smaller than the dots. The grey line corresponds to a fit $\sigma_{NP} \propto T^\alpha$, with $\alpha \approx 0.48$ for $T < 80\text{K}$. At higher temperature σ_{NP} rises with a faster exponent.

to what is commonly seen in good-quality, single-layer graphene devices. r_{NP} was measured at lower temperature in a separate cool-down using a dilution fridge: further lowering T to 400mK increases r_{NP} , at which point it measures $2.3\text{M}\Omega$, then remains constant down to 20mK within experimental error. The full-width at half-maximum in $r_{NP}(V_{BG})$ at 20mK corresponds to a residual impurity density on order 10^{10}cm^{-2} . For carrier densities higher than $\sim 5 \times 10^{10}\text{cm}^{-2}$, r decreases when T is lowered, similarly to what has been observed elsewhere on high-quality samples without a top gate [15] and in our control device [20]. Fig. 2(b) shows $g_{NP}(T)$, which follows a power law $g_{NP} \propto T^\alpha$ as a function of the temperature, with $\alpha = 0.48 \pm 0.05$, as extracted from a linear fit to the curve. This insulating behavior is not due to the opening of a band gap, which would lead to an exponentially-activated conductivity. The tempera-

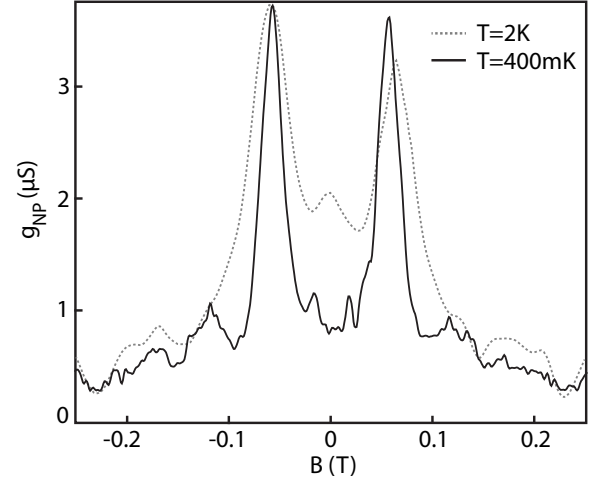


FIG. 3: Conductance at the charge neutrality point g_{NP} as a function of the magnetic field at two different temperatures, $T=2\text{K}$ (dashed grey line) and $T=400\text{mK}$ (black line)

ture dependence is also slower than the T^2 dependence measured in Ref. [17] (and expected from the Boltzmann equation with electron-electron scattering). An evolution similar to ours was reported in suspended graphene [15], although the overall conductance was several orders of magnitude higher.

$g_{NP}(B)$ for $T=2\text{K}$ and 400mK in the range $|B| \leq 250\text{mT}$ exhibits 2 strong peaks located symmetrically at $B = \pm 70\text{mT}$ (Fig. 3). The peak conductance at $\pm 70\text{mT}$ has less T dependence than $g_{NP}(B=0)$. A strong magneto-conductance was seen in Ref. [17] as well and was fit to the weak localization theory for graphene. However, our observed magneto-conductance is distinct from that seen previously in Ref. [17] or in typical two-dimensional conductors in two ways. First the magneto-conductance around $B=0$ has positive curvature, different from the cusp-like, negative curvature typical of WL. Second, after the peak at $\pm 70\text{mT}$, the conductance drops abruptly towards zero, indicating that the device returns to an insulating state. It appears that the magneto-conductance peak is not due to Anderson localization, but rather marks a transition between the zero-field insulating state and the $\nu = 0$ insulator.

To investigate this transition, a low field fan diagram $[g(V_{BG}, B)]$ is measured at $T=2\text{K}$ and shown in Fig. 4(a). Away from the CNP, we observe plateaus for $\nu = 2, 6, 10$ (dashed lines) that are well-developed on the hole side for $B > 0.5\text{T}$. The cut $g(V_{BG}, B=1\text{T})$ shows these plateaus in addition to the $\nu=0$ plateau around the CNP [Fig. 4(c)]. Quantum Hall plateaus are better resolved on the hole side than on the electron side, which we found to be common for two-terminal quantum Hall conductance measurements on other graphene on boron nitride devices. Interestingly, the broken-symmetry $\nu=0$ state seems to persist all the way down to very low fields (solid blue

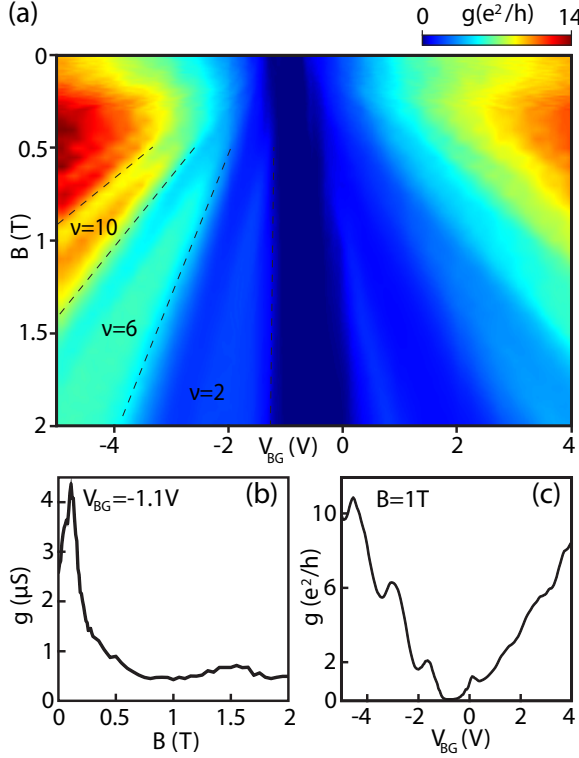


FIG. 4: (a) Conductance g as a function of the transverse magnetic field B and V_{BG} , at $T=2K$, measured in a two probes configuration. The transitions between plateaus are underlined for $\nu=0, 2, 6, 10$. (b) Cut of $g(B)$ at the charge neutrality point $V_{BG} = -1.1V$. (c) Cut of $g(V_{BG})$ at $B=1T$.

region that runs between $V_{BG} \sim 0$ and $-1V$).

Discussion. Typically the disorder in the sample may be extracted from the temperature below which $g(T)$ saturates [5]. The temperature dependence in our device is very strong down to $T \approx 400$ mK, at which point it may remain flat down to 20 mK, the dilution fridge's base temperature, although the temperature dependence in this range is harder to track due to current noise in our setup. The temperature dependence is expected to be flat when $k_B T$ is below the Fermi energy's fluctuations δE_F , allowing us to coarsely estimate δE_F and find an unexpectedly low value $\delta E_F \approx 40 \mu eV$.

Another way to estimate δE_F is to look at the magnetic field at which the $\nu=0$ plateau develops. For our control device [20] the two-terminal conductance develops plateaus at a moderate magnetic field ($\sim 1-2$ T) with value $2e^2/h$ around the CNP (corresponding to $\nu=\pm 2$). In typical graphene-on-BN devices, we and others [33] find that the two-probe conductance at the CNP only starts decreasing from $2e^2/h$ to zero for $B \sim 2-3$ T [20], as the valley degeneracy of the $n=0$ Landau level is lifted [30]. The $\nu=0$ gap is usually fully developed at around 5T, at which point the current becomes unmeasurable with our setup. This is qualitatively different from what we observe with our top-gated de-

vice, where the conductance around the charge neutrality point is never quantized and always very small compared to $2e^2/h$ [Fig. 4(b)]. The conductance is heavily suppressed on the high field side of the conductance peak discussed earlier, corresponding to an opening of the $\nu=0$ gap at ~ 100 mT. In a magnetic field, the energy of Coulomb interactions is on the order $E_C = \frac{e^2}{\epsilon l_B}$, where l_B is the magnetic length $l_B = \sqrt{\frac{\hbar}{eB}}$. While to first order these interactions preserve valley symmetry, it has been shown that higher-order terms break this symmetry and are on order $\delta E_C = \frac{a}{l_B} E_C$, where a is the spacing between neighboring carbon atoms [31–33]. A naive estimate of this contribution gives $\delta E_C \sim 1$ meV/T. Interestingly, the field dependence of the $\nu=0$ gap has been studied in Ref [33], where it was found that the effective g factor $g_{\Delta_0} \equiv d\Delta_0/dB$ for the $\nu=0$ state had this same order of magnitude. We can use this result to estimate the Landau level broadening due to the Fermi level fluctuations from the onset of the $\nu=0$ gap at 100 mT. We find $\delta E_F \sim 100 \mu eV$, in good agreement with our previous estimate based on the low-temperature saturation of $g_{NP}(T)$. This confirms that the Fermi energy fluctuations are at least one order of magnitude lower in our double-gated device than they are in suspended graphene [15, 34].

Using $E_F = \hbar v_F \sqrt{\pi n}$, our inferred fluctuations in E_F correspond to density fluctuations on the order of 10^6 cm^{-2} , two orders of magnitude lower than in most reported suspended devices [34]! The density of impurities is unlikely to be this small, but probably on order 10^9 to $10^{10} cm^{-2}$ [6, 19] and similar to our control device. This is internally consistent: while Coulomb interactions are usually barely screened at the CNP [35], the nearby grounded metallic plane provides additional screening and the Fermi energy fluctuations are therefore expected to be weakened.

The improved screening is likely to be responsible for the diverging resistivity we observe. As charge puddles get shallower and further apart, the minimum conductivity is expected to drop as it becomes harder for electrons to percolate [16, 36]. We note that σ_{NP} was calculated in the percolating regime [36] and predicted to depend on density fluctuations as $\sigma_{NP} \propto \delta n^{0.41}$, a result that may be relevant here as the resistance at p-n boundaries between charge puddles grows to dominate sample resistivity [37]. However, the top gate is tens of nanometers away from the flake, significantly further than reported in Ref. [17], and it is therefore surprising that the screening should have such dramatic consequences, as interactions should naively be screened only on distances larger than the spacing to the top gate. Further work is therefore needed to better understand the role of screening in such systems.

We thank A. Bestwick, P. Gallagher, M. Lee, J. Sanchez-Yamagishi, C. Dean and P. Jarillo-Herrero for

useful technical help and fruitful discussions. This work was supported by the Center on Functional Engineered Nano Architectonics (FENA), the W. M. Keck foundation and the Stanford Center for Probing the Nanoscale (CPN). F. Amet acknowledges support from a Stanford Graduate Fellowship.

-
- [1] Y. Zhang, Y-W. Tan, H. L. Stormer and P. Kim, *Nature* **438**, 201-204 (2005).
 - [2] A. Geim and K. S. Novoselov, *Nature Mat.* **6**, 183-191 (2007).
 - [3] A. F. Young and P. Kim, *Nature Phys.* **5**, 222 (2009).
 - [4] J. Martin, N. Akerman, G. Ulbricht, T. Lohmann, J. H. Smet, K. von Klitzing and A. Yacoby, *Nature Phys.* **4**, 144-148 (2008).
 - [5] K. I. Bolotin, K. J. Sikes, Z. Jiang, M. Klima, G. Fudenberg, J. Hone, P. Kim and H. L. Stormer, *Solid State Comm.* **146**, 351-355 (2008).
 - [6] C. R. Dean, A. Young, I. Meric, C. Lee, L. Wang, S. Sorgenfrei, K. Watanabe, T. Taniguchi, P. Kim, K. Shepard and J. Hone, *Nature Nano.* **5**, 722-726 (2010).
 - [7] K. I. Bolotin, F. Ghahari, M. D. Shulman, H. L. Stormer and P. Kim, *Nature* **462**, 196-199 (2009).
 - [8] C. R. Dean, A. F. Young, P. Cadden-Zimansky, L. Wang, H. Ren, K. Watanabe, T. Taniguchi, P. Kim, J. Hone and K. L. Shepard, *Nature Phys.* **7**, 693-696 (2011).
 - [9] D. C. Elias, R. Gorbachev, A. S. Mayorov, S. V. Morozov, A. A. Zhukov, P. Blake, L. A. Ponomarenko, I. V. Grigorieva, K. S. Novoselov, F. Guinea and A. K. Geim, *Nature Phys.* **7**, 701-704 (2011).
 - [10] D. A. Abanin, S. V. Morozov, L. A. Ponomarenko, R. V. Gorbachev, A. S. Mayorov, M. I. Katsnelson, K. Watanabe, T. Taniguchi, K. S. Novoselov, L. S. Levitov and A. K. Geim, *Science* **332**, 328-330 (2011).
 - [11] J. Nilsson, A. H. Castro Neto, F. Guinea and N. M. R. Peres, *Phys. Rev. Lett.* **97**, 266801 (2006).
 - [12] J. Tworzydło, B. Trauzettel, M. Titov, A. Rycerz and C. W. J. Beenakker, *Phys. Rev. Lett.* **96**, 246802 (2006).
 - [13] J. H. Chen, C. Jang, S. Adam, M. S. Fuhrer, E. D. Williams and M. Ishigami, *Nature Phys.* **4**, 377-381 (2008).
 - [14] Y.-W. Tan, Y. Zhang, K. Bolotin, Y. Zhao, S. Adam, E. H. Hwang, S. Das Sarma, H. L. Stormer and P. Kim, *Phys. Rev. Lett.* **99**, 246803 (2007).
 - [15] K. I. Bolotin, K. J. Sikes, J. Hone, H. L. Stormer and P. Kim, *Phys. Rev. Lett.* **101**, 096802 (2008).
 - [16] S. Adam, E. H. Hwang, V. M. Galitski and S. Das Sarma, *PNAS* **104**(47), 18392-18397 (2007).
 - [17] L. A. Ponomarenko, A. K. Geim, A. A. Zhukov, R. Jalil, S. V. Morozov, K. S. Novoselov, I. V. Grigorieva, E. H. Hill, V. V. Cheianov, V. I. Fal'ko, K. Watanabe, T. Taniguchi and R. V. Gorbachev, *Nature Phys.* **7**, 958-961 (2011).
 - [18] S. Das Sarma, E. H. Hwang and Q. Li, *Phys. Rev. B* **85**, 195451 (2012).
 - [19] J. Xue, J. Sanchez-Yamagishi, D. Bulmash, P. Jacquod, A. Deshpande, K. Watanabe, T. Taniguchi, P. Jarillo-Herrero and B. J. Leroy, *Nature Mat.* **10**(4), 282-285 (2011).
 - [20] Supplementary information
 - [21] A. G. F. Garcia, M. Neumann, F. Amet, J. R. Williams, K. Watanabe, T. Taniguchi and D. Goldhaber-Gordon, *Nano Lett.* **12**(9), 4449-4454 (2012).
 - [22] M. Yamamoto, T. L. Einstein, M. S. Fuhrer and W. G. Cullen, *ACS Nano*, **6**(9), 8335-8341 (2012).
 - [23] J. Velasco Jr, G. Liu, W. Bao and C. N. Lau, *New J. Phys.* **11**, 095008 (2009).
 - [24] R. T. Weitz, M. T. Allen, B. E. Feldman, J. Martin and A. Yacoby, *Science* **330**, 812 (2010).
 - [25] M. T. Allen, J. Martin and A. Yacoby, *Nature Comm.* **3**, 934 (2012).
 - [26] R. V. Gorbachev, A. S. Mayorov, A. K. Savchenko, D. W. Horsell and F. Guinea, *Nano Lett.* **8**(7), 1995-1999 (2008).
 - [27] J. R. Williams, L. DiCarlo and C. M. Marcus, *Science* **317** (5838), 638-641 (2007).
 - [28] B. Huard, J. A. Sulpizio, N. Stander, K. Todd, B. Yang and D. Goldhaber-Gordon, *Phys. Rev. Lett.* **98**, 236803 (2007).
 - [29] S. V. Morozov, K. S. Novoselov, M. I. Katsnelson, F. Schedin, D. C. Elias, J. A. Jaszczak and A. K. Geim, *Phys. Rev. Lett.* **100**, 016602 (2008).
 - [30] Y. Zhang, Z. Jiang, J. P. Small, M. S. Purewal, Y. W. Tan, M. Fazlollahi, J. D. Chudow, J. A. Jaszczak, H. L. Stormer and P. Kim, *Phys. Rev. Lett.* **96**, 136806 (2006).
 - [31] K. Nomura and A. H. MacDonald, *Phys. Rev. Lett.* **96**, 256602 (2006).
 - [32] M. O. Goerbig, *Rev. Mod. Phys.* **83**, 11931243 (2011).
 - [33] A. F. Young, C. R. Dean, L. Wang, H. Ren, P. Cadden-Zimansky, K. Watanabe, T. Taniguchi, J. Hone, K. L. Shepard and P. Kim, *Nature Phys.* **8**, 550556 (2012).
 - [34] A. Mayorov, D. C. Elias, I. S. Mukhin, S. V. Morozov, L. A. Ponomarenko, K. S. Novoselov, A. K. Geim and R. V. Gorbachev, *Nano Lett.* **12** (9), 46294634 (2012).
 - [35] T. Ando, *J. Phys. Soc. Jpn.* **75**, 074716 (2006).
 - [36] V. V. Cheianov, V. I. Fal'ko, B. L. Altshuler and I. L. Aleiner, *Phys. Rev. Lett.* **99**, 176801 (2007).
 - [37] S. Das Sarma, S. Adam, E. H. Hwang and E. Rossi, *Rev. Mod. Phys.* **83**, 407470 (2011)

SUPPLEMENTARY INFORMATION

Device fabrication

Polyvinyl alcohol (2% in water) is spun at 6000 rpm on bare silicon and baked at 160 °C for 5 minutes, resulting in a 40nm thick layer. Then, a layer of PMMA (5% in anisole) is spun at 2400 rpm and baked 5 minutes at 160 °C. The total polymer thickness is on the order of 450nm. Graphene is then exfoliated on this stack using Nitto tape, located using optical microscopy, and characterized with Raman spectroscopy. Boron nitride flakes are exfoliated on a silicon wafer piece with a 300nm thick thermal oxide, then baked in flowing Ar/O₂ at 500 °C to remove tape residue. The cleanliness and thickness of the flakes are characterized with atomic force microscopy and Raman spectroscopy.

The PVA layer is dissolved in deionized water at 90 °C, which lifts-off the PMMA membrane with the graphene attached to it. The membrane is then adhered across a hole in a glass slide [S1] and baked at 110 °C. We then use a home-made probe-station to align the graphene flake on top of the boron nitride substrate. Once both flakes are in contact, the stack is baked at 120 °C to promote adhesion. The PMMA layer is dissolved in hot acetone, then rinsed in IPA, which leaves the graphene flake on top of the boron nitride flake. This stack is annealed in flowing Ar/O₂ at 500 °C for 4 hours, which removes process residue and leaves the graphene flake pristine, as checked by Raman spectroscopy.

We use regular electron beam lithography combined with oxygen plasma etching to pattern a graphene Hall bar. In order to fabricate a suspended top gate above the device, the samples are spin-coated at 6krpm with a solution of polymethyl-methacrylate (950k), 3% in anisole, then baked at 160 °C for 5 minutes. An additional layer of methyl-methacrylate (8.5% in ethyl lactate) is spin-coated at 6krpm and baked 5 minutes at 160 °C. The MMA layer is 50% more sensitive to electron irradiation than the PMMA layer and it is therefore possible to develop the top resist layer without exposing the bottom layer. The e-beam writing system we used is a JEOL 6300, with an acceleration voltage of 100keV. The contacts and the feet of the suspended bridge are exposed with 1000 μ C/cm², which is enough to dissolve both resist layers upon development in MIBK/IPA (1:3) for 45s. The span of the suspended bridge is only exposed with a base dose of 650 μ C/cm², which only develops the top resist layer. After development, the device is cleaned for 2 minutes with UV ozone, then metallized with 1nm of chromium and 200nm of gold.

Figure 5 is a scanning electron micrograph of a graphene on boron-nitride device with a suspended top-gate that has been fabricated using the same recipe. Suspended gates as long as 7 microns have been fabricated

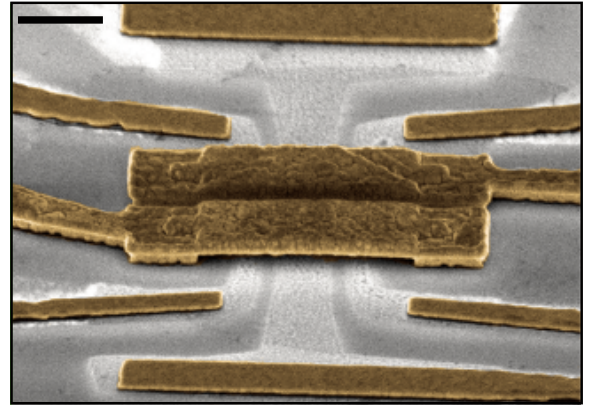


FIG. 5: Scanning electron micrograph of a graphene on boron nitride device with a suspended top gate. Scale bar=1 μ m.

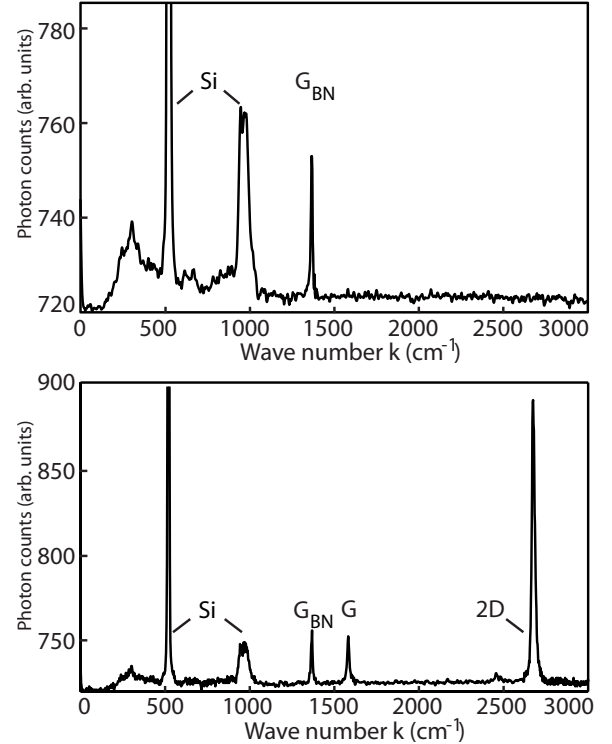


FIG. 6: a) Raman spectrum of the boron nitride flake used for the device described in the main paper, prior to transferring the graphene flake. The boron nitride Raman peak is labelled G_{BN} . b) Raman spectrum of the whole graphene on boron nitride device after oxygen annealing and before contacts were made to the flake. The peaks labelled G and 2D are attributed to graphene.

using this recipe. These usually resist further heat treatment as well as cryogenic temperatures. We found that gate voltages as high as 40V can be applied to the top-gate without damaging it.

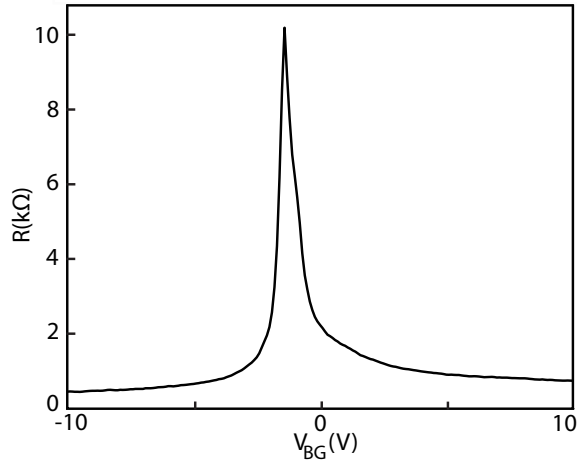


FIG. 7: Resistivity as a function of the back-gate voltage for the control device

Raman spectra

We check the cleanliness of every boron nitride flake we use with atomic force microscopy and Raman spectroscopy. Figure 6.a shows the Raman spectrum of the boron nitride flake used in the device studied in the paper, prior to transferring the graphene flake. The absence of a broad background signal [S2] is a very clear indication that the flake is free of any kind of organic contamination. The Raman spectrum of the transferred device before the last lithographic step -when the suspended gate is patterned, is shown on Figure 6.b. The ratio of the amplitudes of the 2D and G peak is $I_{2D}/I_G = 5.5$, and the full half width of the 2D peak is 19 cm^{-1} , indicating with no ambiguity that the flake studied here is single-layer graphene [S3]. The absence of a broad background signal attests for the cleanliness of the device.

Resistance of a non top-gated sample

The resistivity of a non top-gated part of the sample described in the main paper is shown on figure 7, measured at $T=4\text{K}$. The peak resistivity is $\sim 10\text{k}\Omega$ and does not diverge as the temperature is lowered.

Quantum Hall conductance of a non top-gated device

The two-terminal quantum Hall conductance of a graphene on boron nitride device with no top-gate is shown on Figure 8. The conductance is measured at $T=2\text{K}$ in a two-probe configuration. Most of the measurements in this paper use this geometry, as voltage-biased measurements of the conductance are more convenient than current-biased ones when the device is in-

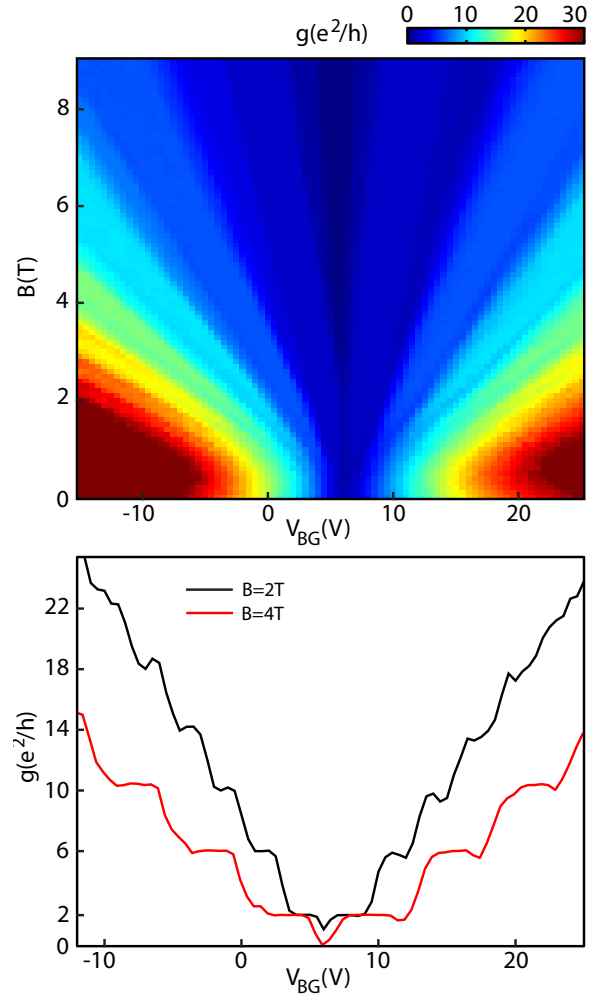


FIG. 8: a) Two terminal inductance as a function of the transverse magnetic field and the back-gate voltage. b) Cuts of the conductance as a function of the back gate voltage at $B=2\text{T}$ (black line) and $B=4\text{T}$ (red line).

ulating, around the charge neutrality point.

As the magnetic field increases, the degeneracy of each Landau level splits and we observe new quantized plateaux. In particular, the $\nu=0$ phase slowly appears around $B=3\text{T}$: this is in sharp contrast with the abrupt transition seen in figure 4b of the main paper, which occurs at a much lower field. Figure 8b shows two sections of the Fan diagram at $B=2\text{T}$ and $B=4\text{T}$. The conductance at 2T shows the standard sequence of plateaux, as seen in other two terminal devices with no splitting of the Landau levels [S4]. We stress that the small dip in conductance at the neutrality point at 2T is only an artifact from the two terminal geometry, as shown in Ref. [S4], and is not related to the opening of the $\nu=0$ gap. At 4T , the device starts being insulating around the charge neutrality point, as the $\nu=0$ gap opens up, and the other plateaux become further resolved.

SUPPORTING REFERENCES

- S1. C. Dean, A. F. Young, I. Meric, C. Lee, L. Wang, S. Sorgenfrei, K. Watanabe, T. Taniguchi, P. Kim, K. L. Shepard and J. Hone, *Nature Nano.* **5**, 722726 (2010)
- S2. A. G. F. Garcia, M. Neumann, F. Amet, J. R. Williams, K. Watanabe, T. Taniguchi and D. Goldhaber-Gordon, *Nano Lett.* **12**(9), 4449-4454 (2012).
- S3. A. C. Ferrari, J. C. Meyer, V. Scardaci, C. Casir-
aghi, M. Lazzeri, F. Mauri, S. Piscanec, D. Jiang,
K. S. Novoselov, S. Roth and A. K. Geim, *Phys.*
Rev. Lett. **97**, 187401 (2006)
- S4. J. R. Williams, D. A. Abanin, L. DiCarlo, L. S. Lev-
itov and C. M. Marcus, *Phys. Rev. B* **80** 045408
(2009)